(e) P. W. Atkins and R. C. Gurd, *Chem. Phys. Lett.*, **16**, 265 (1972); (f) M. S. Child and R. B. Bernstein, *J. Chem. Phys.*, **59**, 5916 (1973); (g) R. G. Gordon, *ibid.*, **51**, 14 (1969); R. W. Redding, *ibid.*, **60**, 1392 (1974); (h) M. Child, *Mol. Phys.*, **28**, 495 (1974); (i) J. B. Delos and W. R. Thorson, *Phys. Rev. A*, **6**, 728 (1972).
(32) For the gap size in the coplanar decomposition of cyclobutane, see J. S. Wright and L. Salem, *J. Amer. Chem. Soc.*, **94**, 322 (1972).
(33) In NaCl, for instance, $\langle\psi_{Ion}|H|\psi_{cov}\rangle$ involves $2\langle\phi_{Cl}|H|\phi_{Na}\rangle$, the one-electron part of which is proportional to the overlap $\langle\phi_{Cl}|\phi_{Na}\rangle$.
(34) (a) L. Salem, *J. Chem. Phys.*, **38**, 1227 (1963), in particular eq 6; (b) L. Salem, *Chem. Phys. Lett.*, **3**, 99 (1969).
(35) The term $\partial V_{ee}/\partial z$, which has been added into (18), vanishes since V_{ee} is purely electronic while z is a nuclear coordinate.
(36) Details of such calculations will be published elsewhere (C. Leforestier, These de 3e Cycle, Orsay, 1975).
(37) An extremely useful reference for the calculation of such integrals is R. F. W. Bader, *Can. J. Chem.*, **40**, 2140 (1962).
(38) For a type A avoided crossing between *two open* shells of different symmetry (k → l and k → m) eq 19 stays true and only the expression for the transition force is slightly different ($F_{A'A''} = \langle l|\partial V/\partial z|m\rangle$).

Calculated Photoionization Cross-Sections and Angular Distributions for the Isoelectronic Series Ne, HF, H_2O, NH_3, and CH_4[1]

Thomas P. Debies and J. Wayne Rabalais*

Contribution from the Department of Chemistry, University of Pittsburgh, Pittsburgh, Pennsylvania 15260. *Received July 13, 1974*

Abstract: Photoionization cross-sections and angular distributions within the orthogonalized plane-wave approximation have been calculated for Ne and the ten-electron first-row hydrides HF, H_2O, NH_3, and CH_4. The calculations are appropriate for photoionization of randomly oriented molecules with an unpolarized photon beam. Three types of cross-sections are presented: (i) specific differential photoionization cross-sections for electrons emitted normal to the photon beam, $\sigma_\perp$, (ii) total differential photoionization cross-sections for electrons ejected normal to the photon beam, $\sigma_\perp{}^{tot}$, and (iii) total photoionization cross-sections for electrons ejected in all directions, σ. Variations in computed cross-sections and asymmetry parameters β as a function of the kinetic energy of the photoelectrons for incident photon energies ranging from threshold to 1500 eV are discussed and possible interpretations are proposed. Relative experimental photoionization band intensities obtained with Ne I, He I, He II, and Mg Kα radiation sources and asymmetry parameters β obtained with He I radiation are compared with computed $\sigma_\perp$ and β values.

I. Introduction

The photoionization cross-sections of the ten-electron first-row hydrides CH_4, NH_3, H_2O, and HF are of fundamental importance in studies of atmospheric and astrophysical processes and in analysis of photoelectron spectral (PES) band intensities. Photoabsorption of vacuum ultraviolet solar radiation leading to photodissociation and photoionization plays a significant part in the heating and structure of the atmospheres. It is directly responsible for the ionosphere and contributes significantly to molecular dissociation and heating of the atmosphere above 100 km.[2] Since all gases have high photoabsorption cross-sections in the short wavelength end of the spectrum, it is expected that similar processes take place in planetary atmospheres other than that of the earth. CH_4, NH_3, and H_2O are common constituents of the atmospheres and although HF is not as common, traces of it have been observed in the atmosphere of Venus.[3] With regards to PES, it is possible to use the variation in differential photoionization cross-sections as a function of energy of the incident photons as a criterion for spectral assignments.[4] The ability to predict photoionization cross-sections is very important in PES, for spectral assignments should be consistent with regards to intensity as well as energy analysis of the bands.

In this paper we present the calculated differential photoionization cross-sections and angular distribution parameters for the ten-electron first-row hydrides and neon and compare these with the corresponding relevant experimental quantities. Three different types of cross-sections are presented. (1) The *specific differential photoionization cross-section* $(d\sigma/d\Omega)_j$ *is a measure of the number of electrons emitted from orbital j per unit time per unit solid angle* Ω. Since the most common experimental arrangement involves randomly oriented molecules and collection of photoelectrons through a slit centered normal to an incident unpolarized photon beam, we have calculated the corresponding averaged specific differential cross-section, henceforth referred to as $\sigma_\perp$. (2) The *total differential cross-section* $\sigma_\perp{}^{tot}$ *has been calculated as the sum of the specific differential cross-sections for the experimental conditions described in case 1, i.e.* $\sigma_\perp{}^{tot} = \sum_i \sigma_{\perp i}$ *where i represents a summation over all occupied orbitals.* (3) *The total specific cross-section* σ *is a measure of the number of electrons emitted from an orbital per unit time in all directions.* We have calculated the averaged σ corresponding to randomly oriented molecules and unpolarized incident photons. In order to observe the dependence of $\sigma_\perp$ and $\sigma_\perp{}^{tot}$ on photon energy, calculations were performed for various photon energies between threshold and 1500 eV; plots of $\sigma_\perp$ and $\sigma_\perp{}^{tot}$ *vs.* incident photon energy are presented for Ne, HF, H_2O, NH_3, and CH_4. These cross-sections are compared to relative experimental band intensities as obtained from Ne I, He I, He II, and Mg Kα radiation sources. The σ and the angular distribution parameter β are computed only for the four sources listed above. The calculated β values are compared to those obtained from experimental determinations using a He I radiation source.

The cross-sections and angular distributions are calculated in the plane-wave (PW) and orthogonalized plane-wave (OPW) approximations according to the theoretical equations derived by Ellison[5] and applied by Rabalais, *et al.*[6,7] Some of the most important elements of a cross-section cal-

culation are the initial and final state wave functions, the latter containing a one-electron function representing the ionized electron. A plane-wave PW is the easiest and simplest approximation to this one-electron continuum function and serves as a useful first approximation for the cross-section.[8-10] The PW approximation is known to be inaccurate near threshold. It can be improved by Schmidt orthogonalization of the PW to the occupied ground-state bound orbitals, hence the OPW approximation.[5-7,11] The OPW helps to reflect the influence of the attractive molecular potential on the outgoing electron.

In section II we discuss the theoretical concepts and equations used in calculating the cross-sections and angular distributions. Section III is a brief description of the experimental measurements of photoelectron band intensities. Section IV is a discussion of the results obtained from $\sigma_\perp$ and β computations. In section V, we consider the $\sigma_\perp{}^{tot}$ and σ results. The conclusions are summarized in section V.

II. Theoretical Method

A. Photoionization Cross-Sections. The expression for the differential cross-section for production of photoelectrons in the solid angle $d\Omega$ is[5]

$$\frac{d\sigma}{d\Omega} = \frac{\pi e^2}{m^2\omega c} |\mu \cdot \langle \Psi_0 | \Sigma p_n | \Psi_j \rangle|^2 \rho(E) \quad (1)$$

We define the initial state Ψ_0 as a Slater determinant of doubly occupied orthonormal MO's ϕ_l. The final state Ψ_j must be representative of the molecular ion and the free electron; using the frozen orbital approximation, Ψ_j is given as a linear combination of two Slater determinants resulting in a spin singlet in which one electron has been promoted from the MO ϕ_j to an unbound normalized plane-wave orbital

$$|\mathrm{PW}(k)\rangle = L^{-3/2} e^{ik\cdot r} \quad (2)$$

where L is the edge length of a large cubic box. The magnitude of the wavevector k and the resulting density of states ρ are

$$k = [2m(\hbar\omega - \mathrm{IP}_j)]^{1/2}/\hbar \quad (3)$$

and

$$\rho(E) = mkL^3/(2\pi^2\hbar^2) \quad (4)$$

respectively, where IP_j is the ionization potential of MO ϕ_j. Substituting eq 2 and 4 into eq 1 yields

$$\frac{d\sigma}{d\Omega} = \frac{e^2 k L^3}{2\pi m c \hbar^2 \omega} |\mu \cdot P_{0j}|^2 \quad (5)$$

where the quantity within the absolute value signs is the dot product of the polarization vector μ of the incident radiation with the transition moment integral P_{0j}. Since the plane-wave is an eigenfunction of the momentum operator $p_n = (\hbar/i)\nabla$ with eigenvalue $\hbar k$, P_{0j} can be expressed as

$$P_{0j} = 2^{1/2}\hbar\left[k\langle\phi_j|\mathrm{PW}(k)\rangle + i\sum_l \langle\phi_j|\nabla|\phi_l\rangle\langle\phi_l|\mathrm{PW}(k)\rangle\right] \quad (6)$$

Terms with $l = j$ may be omitted from the summation over occupied MO's ϕ_l since the mean value of the electron momentum is zero for bound states. The important point concerning eq 6, as emphasized by Lohr,[11] is that it represents the unbound electron not as a simple plane-wave (PW) but as *a plane-wave which is orthogonalized (OPW) to all occupied MO's* ϕ_l. The LCAO (linear combination of atomic orbitals) approximation is used for the MO's with the initial basis χ_μ defined as Slater type atomic orbitals (STO's). Since the analysis is heavily dependent on rotations and properties of angular momentum, it is expeditious to transform to a complex AO basis defined with angular factors as spherical harmonics.

The basic components in eq 6 are the overlap integrals connecting the AO χ_p with the plane-wave PW(k) and the gradient matrix elements connecting MO's ϕ_j and ϕ_l. The plane-wave can be expressed[5] in terms of the coupling equations for spherical harmonics $Y_{l,m}$ and Raleigh's expansion into spherical Bessel functions. The resulting overlap integral contains spherical Bessel functions and STO's. The gradient elements are related to a linear combination of components of transition moments connecting the MO ϕ_j with all other occupied MO's ϕ_l.

The expansion of eq 5 and 6 and derivation of the components are detailed in ref 1-3; only a brief summary is presented here. The square of the dot product between the polarization vector and the transition moment $|\mu\cdot P_{0j}|^2$ yields real and imaginary components of overlap integrals and gradient elements. These components are expressed in terms of spherical harmonics $Y_{l,m}$, spherical Bessel functions $j_\lambda(kR)$, Clebsch-Gordon coefficients $C(l'l''l; m'm'')$, Γ functions $\Gamma(x)$, and complex STO basis functions. Since the most frequently employed experimental arrangement involves a gaseous sample (randomly oriented molecules) and collection of photoelectrons through a slit centered normal to an incident unpolarized photon beam, we have calculated the corresponding average differential cross-section $\sigma_\perp$.[6] This involves averaging over all space defined by the Euler angles and over all polarization angles of the incident radiation.

A computer program for the entire calculation is formulated with the ultimate input consisting of the real AO basis χ_μ, the LCAO-MO coefficients, the molecular coordinates for each atom in the polyatomic, the energy $\hbar\omega$ of the exciting radiation, and the ionization energy IP_j of the occupied MO's ϕ_l. We used experimental molecular coordinates appropriate to the neutral molecule ground states and experimental ionization energies. Molecular wave functions were all of the *ab initio* SCF-LCAO-MO type employing minimal bases of nonorthogonal real Slater-type orbitals;[12-14] orbital exponents ζ were chosen according to Slater's rules.

B. Angular Distributions. The differential cross-section $d\bar{\sigma}/d\Omega$ for linearly polarized light and randomly oriented molecules is expressed in either of the two alternative forms in terms of the total cross-section σ and the asymmetry parameter β[7]

$$d\sigma/d\Omega = (\bar{\sigma}/4\pi)[1 + \tfrac{1}{2}\beta(3\cos^2\theta_k - 1)] \quad (7)$$

$$= (\bar{\sigma}/4\pi)[1 + \tfrac{1}{2}\beta(3\sin^2\theta_k''\cos^2\phi_k'' - 1)] \quad (8)$$

where θ_k is the angle between the propagation vector k of the ejected electron and the electric vector μ of the exciting radiation and (θ_k'', ϕ_k'') are polar coordinates of k using the photon beam as a polar axis. Since $d\bar{\sigma}/d\Omega \geq 0$, it follows that $2 \geq \beta \geq -1$. For unpolarized light, eq 8 is averaged over all orientations of μ, *i.e.*, $0 \leq \phi_k'' \leq 2\pi$, to give

$$\langle\bar{\sigma}\rangle_{Av} = \langle d\bar{\sigma}/d\Omega\rangle_{Av} = (\sigma/4\pi)[1 - \tfrac{1}{4}\beta(3\cos^2\theta_k'' - 1)] \quad (9)$$

Here, $\beta = 2$ corresponds to a pure $\sin^2\theta_k''$ distribution, $\beta = 0$ corresponds to an isotropic distribution, and $\beta = -1$ corresponds to a $(1 + \cos^2\theta_k'')$ distribution. The averaged differential cross-section for collection of electrons normal to the incident unpolarized photon beam is

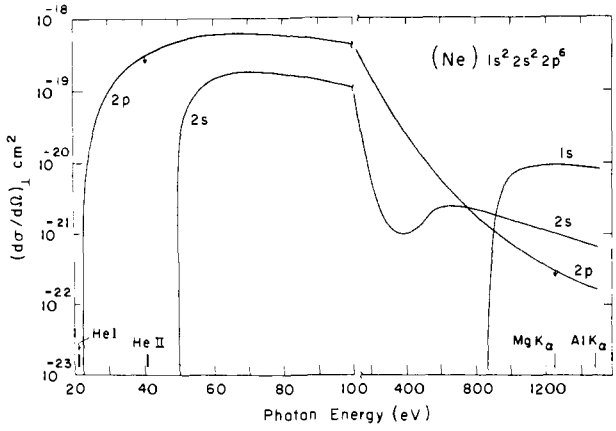

Figure 1. Specific differential photoionization cross-section $\sigma_\perp$ of Ne as a function of incident photon energy.

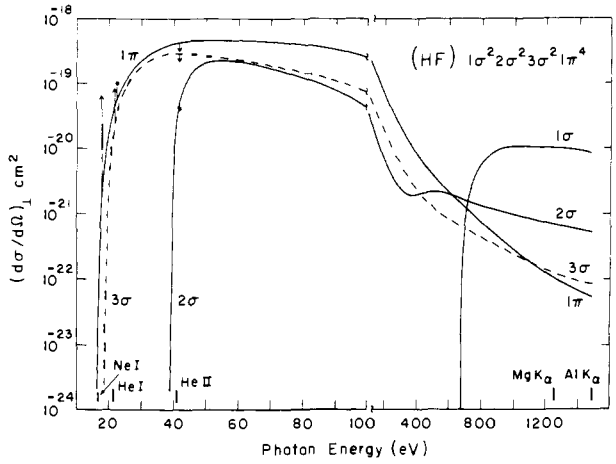

Figure 2. Specific differential photoionization cross-section $\sigma_\perp$ of HF as a function of incident photon energy.

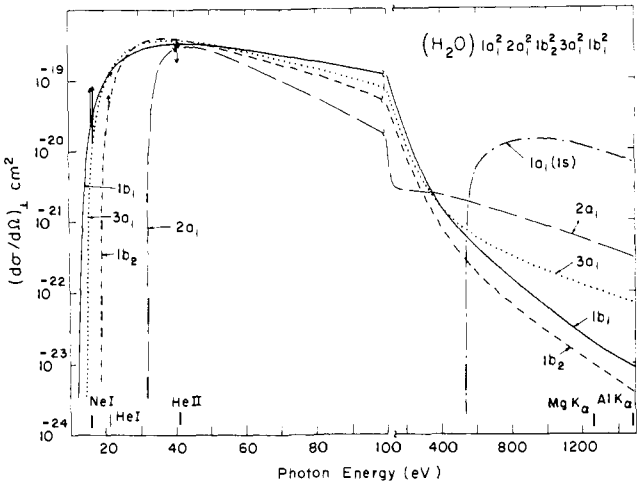

Figure 3. Specific differential photoionization cross-section $\sigma_\perp$ of H_2O as a function of incident photon energy.

$$\sigma_\perp = \langle\bar{\sigma}\rangle_{Av,\perp} = (\sigma/4\pi)(1 + \tfrac{1}{4}\beta)\ \theta_k'' = \pi/2 \qquad (10)$$

The β and σ are calculated along with $\sigma_\perp$ from the computer programs of the previous section. The specific equations for obtaining β's and σ's are outlined in our previous papers.[5-7]

III. Experimental Aspects

The uv photoelectron spectra were measured on a Perkin-Elmer Model PS-16 spectrometer modified for use with Ne I (736 Å), He I (584 Å), and He II (304 Å) resonance radiation sources. The spectrometer uses an electrostatic deflection analyzer which accepts photoelectrons through a 0.006 in. wide slit centered at right angles to the incident radiation.

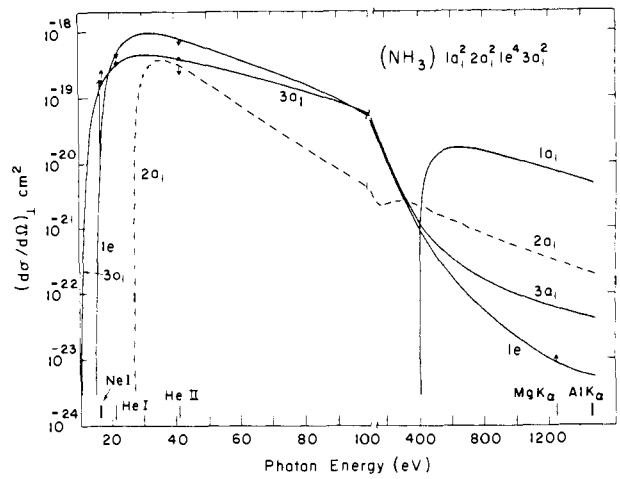

Figure 4. Specific differential photoionization cross-section $\sigma_\perp$ of NH_3 as a function of incident photon energy.

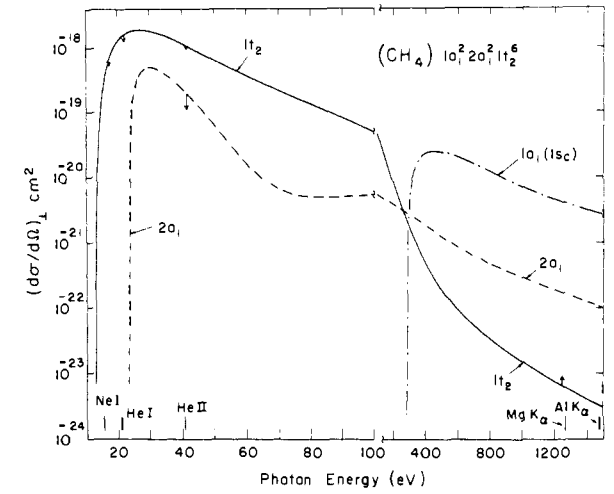

Figure 5. Specific differential photoionization cross-section $\sigma_\perp$ of CH_4 as a function of incident photon energy.

Photoelectron spectra were recorded for the three uv excitation sources described above. The relative band intensities were determined as A/E[6,15,16] where A is the total area of the band obtained by integrating over all its vibrational components by means of a Hruden planimeter and E is the electron kinetic energy at the band maximum. The intensities obtained in this manner are only first-order approximations to the true line intensities for they neglect autoionization phenomena and changes in molecular geometry and vibronic interaction upon ionization.

Relative line intensities of bands produced by X-radiation were obtained by integrating the peaks in the gas-phase spectra of Siegbahn, *et al.*[17] These spectra were obtained on a double focusing magnetic deflection spectrometer. Corrections for variation in kinetic energy of the photoelectrons were not made, although such corrections for this type of analyzer are expected to be small.

IV. Specific Differential Cross-Sections and Angular Distributions

The plane-wave (PW) approximation was used to calculate $\sigma_\perp$ for photon energies ranging from threshold to 1500 eV. Plots of $\sigma_\perp$ *vs.* $\hbar\omega$ are shown in Figures 1-5 for ionization of electrons from the filled orbitals of Ne, HF, H_2O,

Table I. Principal Maxima in Atomic Orbital Cross-Sections as a Function of Electron Energy for Best Atom STO's[a]

Atom	STO	Principal max, eV	Atom	STO	Principal max, eV
H	1s	8	F	1s	585
				2s	25
C	1s	265		2p	60
	2s	10			
	2p	24	Ne	1s	685
				2s	30
N	1s	365		2p	72
	2s	15			
	2p	36	O	1s	485
				2s	20
				2p	48

[a] Best atom Slater type orbitals are obtained from E. Clementi, *IBM, J. Res. Develop., Suppl.*, **9**, 2 (1965).

NH_3, and CH_4. Due to the longer computer times required, *the orthogonalized plane-wave (OPW) calculations were carried out only at those photon energies for which we have excitation sources available: 16.7, 21.2, 40.8, and 1253 eV. The corrections which the OPW places on the PW method are indicated as arrows at the appropriate energies in Figures 1–5.* For some curves, no arrows are indicated at these energies because the OPW correction is negligible.

A. General Shapes of the Cross-Section Curves. The cross-sections rise sharply near the ionization threshold, go through a maximum (or in some cases maxima), and then decrease (usually monotonically) to small values for excitation energies much greater than the ionization threshold. The initial maximum in the cross-section curves, sometimes called the "spectral head," is located at $\hbar\omega \simeq (2.0 \pm 0.5)$IP, where IP is the ionization threshold. The rise to the maximum at the ionization threshold is much too slow in these plane-wave calculations, for it is known that experimental cross-sections behave more like step functions at the threshold.

Calculated cross-sections do not all decrease monotonically after going through an initial maximum; in many cases, there are additional maxima and minima or changes in curvature that occur at increasing photon energies. The two possible sources for these maxima and minima are the spherical Bessel functions and the atomic orbital composition of the MO ionized. The spherical Bessel functions are strongly damped and small compared to unity after going through their initial minima or maxima. They exert their greatest influence on intensities only at very low photon energies, *i.e.*, close to the threshold. In fact, at high values of k, *e.g.*, $k > \sim 60$ eV, we find that two-center contributions to the cross-section become negligible compared to one-center contributions. Thus, the curves are best understood in terms of one-center contributions, *i.e.*, the overlap integral of the AO with the PW multiplied by the net population of AO χ_p in MO ϕ_j. Using best atom STO's, it can be shown that elements display characteristic maxima in their AO cross-section corresponding to the energy at which the AO–PW overlap is maximized. The principal maxima in the AO cross-sections for Ne, F, O, N, C, and H are listed in Table I. As noted, contributions of AO cross-sections to an MO cross-section are regulated by the net population $|c_{jp}|^2$ of the AO χ_p in the MO ϕ_j. We would expect to see distinct maxima only from AO's which have comparable populations and which have "characteristic maxima" that are sufficiently separated.

The initial maxima in the curves occur at low photon energies. At high photon energies many of the curves exhibit additional maxima or changes in curvature. These high-energy fluctuations are best understood in terms of individual AO cross-sections. As noted in our previous work,[5] relative cross-sections of MO's in the high-energy region are mainly determined by their 1s character since $\sigma_{1s} \gg \sigma_{2s}$ or σ_{2p}. These inner 1s electrons display characteristic maxima at several hundred electron volts (Table I); thus, for large values of the wave-vector k, the magnitude of the overlap with the PW is much greater for 1s than for 2s or 2p AO's. The σ (or a) type MO's all have a small admixture of 1s AO character. *Therefore, even though the intensities of σ and π valence MO's are comparable in the low-energy region, the small amount of 1s character is sufficient to make σ MO's more intense than π MO's in the soft X-ray region notwithstanding the twofold degeneracy of π MO's.* This distinction between σ and π MO's is not an artifact of the LCAO or plane-wave approximations.[18] The σ and a type MO's in Figures 1–5 all have small amounts of 1s-core forced hybridization, which sometimes yield high-energy maxima and which always yield higher cross-sections than π, b, or t MO's in which 1s core is absent.

B. Orthogonalized Plane-Wave Contributions. Inspection of eq 6 shows that the PW contribution contains a factor k which is absent in the OPW contribution. Thus, for high k, the OPW corrections become small compared to the PW terms. For very small k, the OPW may strongly correct the calculated PW curves so that they more closely approximate the step function that is observed experimentally. These trends are visual in Figures 1–5. The OPW terms all contain gradient elements $\langle\phi_j|\nabla|\phi_l\rangle$, related to bound–bound dipole transition probabilities connecting the ionized MO ϕ_j and a different occupied MO ϕ_l. *Thus, we have a "selection rule" for OPW contributions: the cross-section for photoionizing an electron from ϕ_j will be modified by orthogonalization of the PW to all occupied MO's ϕ_l which combine with ϕ_j under a dipole operator.*

Near threshold, the largest OPW corrections arise from the overlap of the plane-wave with valence orbitals, $\langle\phi_l|\mathrm{PW}(k)\rangle$. The OPW correction is sometimes larger than the PW contribution in this region. For high electron energies, *i.e.*, for above threshold, the largest values of the overlap integral occur with core orbitals. However, as stated above, the OPW corrections are usually small in the soft X-ray region. In fact, *significant OPW corrections to a valence MO in the soft X-ray region occur only when there is an intense bound–bound dipole transition (e.g., 1s ↔ 2p) connecting a given valence MO ϕ_j with a core MO ϕ_l.*

C. Angular Distributions. The asymmetry parameter β and the total specific cross-section σ_j for ionization from specific MO's at various photon energies are presented in Table II. The total σ at any given photon energy is simply a sum of the specific σ_j's. Our calculations yield large variations in β as a function of photon energy. Most of these variations can be interpreted in terms of two distinct approaches. (i) *β can be correlated with the most probable value of the angular momentum quantum number l of the MO being ionized.*[7,19,20] It is found that at high photon energies, $\beta = 2$ for $l = 0$ but approaches a lower value, 0 or -1, for $l = 1$. (ii) *Deflections of β from 2, i.e., the β obtained from the PW approximation, can be related to OPW corrections of the PW approximation.*[7] In this approach, deviations of β from 2 can be predicted from the significant OPW contributions.

D. Comparison of Theory and Experiment. Relative experimental band intensities and calculated differential photoionization cross-sections $\sigma_\perp$ are compared in Table III. Agreement between calculated and relative experimental intensities is satisfactory. It is well known that the PW approximation is rather crude when the electron kinetic energy is low; the OPW correction helps to reflect the influence

Table II. Total Specific Photoionization Cross-Sections σ and Asymetry Parameters β for Ne and the Frst-Row Hydrides

Molecule	Assignment[b]		IP, eV[b]	Theoretical σ[a] and β — Ne I (16.8 eV) σ[c]	Ne I (16.8 eV) β	He I (21.2 eV) σ[c]	He I (21.2 eV) β	β(exptl)[e]	He II (40.8 eV) σ[c]	He II (40.8 eV) β	Mg Kα (1254 eV) σ[d]	Mg Kα (1254 eV) β
Ne	(2p)	^2P	22.0						0.843	0.785	2.57	0.719
	(2s)	^2S	49.0								7.64	2.00
	(1s)	^2S	870.0								80.6	2.00
HF	(1π)	$^2\pi$	16.1	0.442	−0.086	1.02	0.104		3.23	1.73	0.969	1.18
	(3σ)	$^2\Sigma$	18.6 (A) 19.5 (V)			0.979	0.221		1.98	1.61	1.09	1.66
	(2σ)	$^2\Sigma$	39.0 (V)						0.394	1.38	6.14	2.00
	(1σ)	$^2\Sigma$	686								78.4	2.00
H_2O	($1b_1$)	$^2B_1$	12.6	1.16	−0.382	1.28	0.319	1.0 ± 0.1	2.29	1.74	0.234	0.0596
	($3a_1$)	$^2A_1$	13.8 (A) 14.7 (V)	1.14	−0.269	1.35	0.311	0.3 ± 0.1	2.59	1.79	0.931	1.69
	($1b_2$)	$^2B_2$	17.2 (A) 18.5 (V)			0.893	−0.301	−0.1 ± 0.2	2.29	1.77	0.108	0.358
	($2a_1$)	$^2A_1$	32.2 (V)						1.48	1.96	3.96	2.00
	($1a_1$)	$^2A_1$	540								76.2	2.00
NH_3	($3a_1$)	$^2A_1$	10.2 (A) 10.9 (V)	2.35	1.23	3.37	1.68		3.37	1.95	0.517	1.90
	(1e)	^2E	15.0 (A) 16.0 (V)	1.38	−0.337	2.09	0.656		2.94	1.86	0.056	1.78
	($2a_1$)	$^2A_1$	27.0 (V)						1.98	1.69	2.48	2.00
	($1a_1$)	$^2A_1$	406								59.0	2.00
CH_4	($1t_2$)	$^2T_2$	12.6 (A) 14.0 (V)	5.75	0.614	10.9	1.61	0.6 ± 0.1	8.36	1.95	0.0985	0.441
	($2a_1$)	$^2A_1$	23.0 (V)						0.955	1.93	1.39	2.00
	($1a_1$)	$^2A_1$	290								37.0	2.00

[a] The σ values include degeneracy factors for the orbital ionized. [b] Ionic states and ionization potentials corresponding to photoelectron transitions. A = adiabatic IP; V = vertical IP; no letter indicates A = V. [c] Total specific photoionization cross-section in units of 10^{-18} cm^2. [d] Total specific photoionization cross-section in units of 10^{-21} cm^2. [e] Reference 20.

of the attractive molecular potential. Nevertheless, the steep slopes in $\sigma_\perp$ *vs.* $\hbar\omega$ at low electron energy render the possibility of large errors in comparing relative intensities. In general, agreement between experiment and theory improves as $\hbar\omega$ increases above threshold.

Nearly all experimental measurements of β have been obtained with He I excitation. It is just in this region that the computed β is changing rapidly with photon energy. Also, of course, the OPW approximation does not properly reflect the attractive molecular potential, the influence of which is greatest near threshold. In spite of these reservations, comparison between calculated and experimental β for He I as displayed in Table II is not discouraging. It will be interesting to see if the calculated features approach ex-

Table III. Specific Differential Photoionization Cross-Sections $\sigma_\perp$ and Relative Experimental Intensities[a] of Ne and the First-Row Hydrides

Molecule	Assignment		IP, eV[b]	Specific differential photoionization cross-sections $\sigma_\perp$ — Ne I (16.8 eV) Exptl	Ne I (16.8 eV) Theor[c]	He I (21.2 eV) Exptl	He I (21.2 eV) Theor[c]	He II (40.8 eV) Exptl	He II (40.8 eV) Theor[c]	Mg Kα (1254 eV) Exptl	Mg Kα (1254 eV) Theor[d]
Ne	(2p)	^2P	22.0						2.41	0.02	2.41
	(2s)	^2S	49.0							0.04	9.13
	(1s)	^2S	870							1.00	96.2
HF	(1π)	$^2\Pi$	16.1		0.682		1.08	1.00	3.19		0.90
	(3σ)	$^2\Sigma$	18.6 (A) 19.5 (V)				0.821	0.41	2.19		1.23
	(2σ)	$^2\Sigma$	39.0						0.421		7.37
	(1σ)	$^2\Sigma$	686								93.6
H_2O	($1b_1$)	$^2B_1$	12.6	0.81	0.834	0.85	1.10	0.96	2.62	0.095	0.189
	($3a_1$)	$^2A_1$	13.8 (A) 14.7 (V)	1.0	0.845	1.0	1.15	1.0	2.98	0.26	1.05
	($1b_2$)	$^2B_2$	17.2 (A) 18.5 (V)			0.85	0.657	0.80	3.17	0.081	0.0933
	($2a_1$)	$^2A_1$	32.2 (V)						1.75	1.0	4.72
	($1a_1$)	$^2A_1$	540							19	91.0
NH_3	($3a_1$)	$^2A_1$	10.2 (A) 10.9 (V)		2.44	1.00	3.82	1.00	4.00		0.06
	(1e)	^2E	15.0 (A) 16.0 (V)		2.18	2.20	3.92	1.90	6.86		0.11
	($2a_1$)	$^2A_1$	27.0 (V)						2.24		2.92
	($1a_1$)	$^2A_1$	406								70.4
CH_4	($1t_2$)	$^2T_2$	16.2 (A) 14.0 (V)		5.29		12.2	10	9.91	0.27	0.0873
	($2a_1$)	$^2A_1$	23.0 (V)					1.4	1.13	1.0	1.67
	($1a_1$	$^2A_1$	290							20	44.1

[a] The Ne I, He I, and He II spectra of H_2O, NH_3, and CH_4 were obtained in this laboratory. Band intensities were determined from the average of three spectra as A/E (see text) and normalized such that the intensity of one of the bands is unity. The He I intensities for HF were measured from the spectra of C. R. Brundle, *Chem. Phys. Lett.*, **7**, 317 (1970). The Mg Kα intensities were measured from the spectra of ref 17. [b] A = adiabatic IP; V = vertical IP; no letter indicates that A = V. [c] $\sigma_\perp$ in units of 10^{-19} cm^2. [d] $\sigma_\perp$ in units of 10^{-22} cm^2.

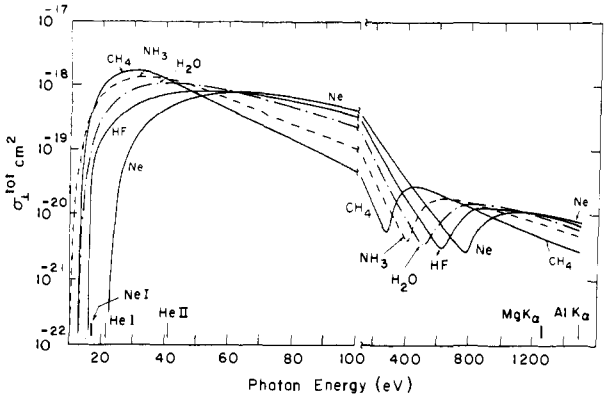

Figure 6. Total differential cross-section $\sigma_\perp^{tot}$ of Ne, HF, H_2O, NH_3, and CH_4 as a function of incident photon energy.

periment more closely as excitation energy increases; however, experimental molecular β determinations are not yet available with high photon energies. Certainly, β can be an important parameter for identifying transitions if we can reproduce it theoretically.

V. Total Differential $\sigma_\perp^{tot}$ and Total σ Cross-Sections

Plots of the total differential cross-section $\sigma_\perp^{tot}$ *vs.* $\hbar\omega$ are shown in Figure 6 for ionization of electrons from the filled orbitals of Ne and the first-row hydrides. The cross-sections in these curves are a sum of the specific differential cross-sections for each molecule in Figures 1–5.

The low energy $\sigma_\perp^{tot}$ maximum ($\hbar\omega < 60$ eV) is due to the maximum in the sum of the valence MO $\sigma_\perp$'s. As noted earlier, the maximum in this region is due to the overlap of 2s and 2p and hydrogen 1s AO's with the PW. As expected from Table I, this maximum shifts to higher energies with the increasing atomic number of the central atom. The value of the maximum decreases progressively across the series $CH_4 > NH_3 > H_2O > HF > Ne$. This trend is a result of two factors: (i) the number of hydrogen AO's in the molecule is significant in this region because of their low energy principal maximum (Table I); (ii) the radial extent of the 2s and 2p AO's in the valence MO's increases as $Ne < F < O < N < C$, providing a larger cross-section.

In the region 50–80 eV the curves cross each other resulting in an inversion of the lower energy ordering. This ordering remains inverted until the region of the 1s ionization energies is reached. In this high-energy region, the $\sigma_\perp^{tot}$ are determined mainly by the 1s, 1σ, or $1a_1$ MO which is essentially a central atom 1s core AO. The position of the maximum in this region moves to higher energy as the atomic number of the central atom increases, in accord with expectations from Table I. As in the low-energy region, the intensity of this maximum increases with decreasing atomic number of the central atom. However, at the excitation energies used in X-ray electron spectroscopy (1254 and 1486 eV), the $\sigma_\perp^{tot}$ increase with increasing atomic number. The total cross-sections σ listed in Table II exhibit similar trends as the $\sigma_\perp^{tot}$.

It is obvious from the above discussion that the molecule with the highest cross-section in one spectral region may have the lowest cross-section in some other region and that these relative intensities change in a complex manner.

VI. Conclusions

We have shown that the PW approximation is useful for understanding *variations* in the photoionization cross-sections and asymmetry parameters as a function of photon energy. The OPW corrections to the PW approximation are most significant near the ionization threshold where the electron kinetic energy is low; the PW method is generally adequate (within at most 15%) when photon energies are much greater than threshold. Agreement between calculated and realtive experimental band intensities is satisfactory in the soft X-ray region, but somewhat poorer in the uv region. The deficiency in the uv region is due to the inadequacy of the OPW approximation near threshold. Agreement between calculated and experimental β values for He I excitation is marginal; we expect better agreement in the soft X-ray region; however, experimental β values for this region are not presently available.

References and Notes

(1) Supported by the U. S. Army Research Office.
(2) G. V. Marr, "Photoionization Processes in Gases," Academic Press, New York, N. Y., 1967.
(3) (a) P. Connes, J. Connes, W. S. Benedict, and L. D. Kaplan, *Astrophys. J.*, **147**, 1231 (1967); (b) G. P. Kuiper and F. F. Forbes, *Commun. Planet Lab.*, **6**, 177 (1967).
(4) A. Katrib, T. P. Debies, R. J. Colton, T. H. Lee, and J. W. Rabalais, *Chem. Phys. Lett.*, **22**, 196 (1973).
(5) F. O. Ellison, *J. Chem. Phys.*, **61**, 507 (1974).
(6) J. W. Rabalais, T. P. Debies, J. L. Berkosky, J. T. J. Huang, and F. O. Ellison, *J. Chem. Phys.*, **61**, 516 (1974).
(7) J. W. Rabalais, T. P. Debies, J. L. Berkosky, J. T. J. Huang, and F. O. Ellison, *J. Chem. Phys.*, **61**, 529 (1974).
(8) I. G. Kaplan and A. P. Markin, *Opt. Spectrosc. (USSR)*, **24**, 475 (1958); **25**, 275 (1968).
(9) L. L. Lohr and M. B. Robin, *J. Amer. Chem. Soc.*, **92**, 7241 (1970).
(10) W. Thiel and A. Schweig, *Chem. Phys. Lett.*, **12**, 49 (1971); **16**, 409 (1972); **21**, 541 (1973); *J. Chem. Phys.*, **60**, 951 (1974).
(11) L. L. Lohr, Jr., "Electron Spectroscopy," D. A. Shirley, Ed., North-Holland Publishing Co., Amsterdam, 1972, p 245–258.
(12) W. E. Palke and W. N. Lipscomb, *J. Amer. Chem. Soc.*, **88**, 2384 (1966).
(13) B. J. Ransil, *Rev. Mod. Phys.*, **32**, 245 (1968).
(14) S. Aung, R. M. Pitzer, and S. I. Chan, *J. Chem. Phys.*, **49**, 2071 (1968).
(15) O. Klemperer, "Electron Optics," Cambridge University Press, London, 1953, pp 408–411.
(16) J. Berkowitz and P. M. Guyon, *Int. J. Mass Spectrom. Ion Phys.*, **6**, 302 (1971).
(17) K. Siegbahn, *et al.*, "ESCA Applied to Free Molecules," North-Holland Publishing Co., Amsterdam, 1971.
(18) The 1s character in the valence orbitals arises from the use of properly orthogonalized Slater AO's. For details see: J. T. J. Huang, F. O. Ellison, and J. W. Rabalais, *J. Electron Spectrosc.*, **3**, 339 (1974).
(19) M. O. Krauss, *Phys. Rev.*, **177**, 151 (1968).
(20) T. A. Carlson, G. E. McGuire, A. E. Jonas, K. L. Cheng, C. P. Anderson, C. C. Lu, and B. P. Pullen, "Electron Spectroscopy," D. A. Shirley, Ed., North-Holland Publishing Co., Amsterdam, 1972, p 207.